



**HAL**  
open science

## Progress in calibration-free laser-induced breakdown spectroscopy

Jörg Hermann, Christoph Gerhard, Miloš Burger, Valentin Craciun, Frédéric Pelascini

► **To cite this version:**

Jörg Hermann, Christoph Gerhard, Miloš Burger, Valentin Craciun, Frédéric Pelascini. Progress in calibration-free laser-induced breakdown spectroscopy. *Spectrochimica Acta Part B: Atomic Spectroscopy*, 2022, pp.106595. 10.1016/j.sab.2022.106595 . hal-03902732

**HAL Id: hal-03902732**

**<https://hal.science/hal-03902732v1>**

Submitted on 16 Dec 2022

**HAL** is a multi-disciplinary open access archive for the deposit and dissemination of scientific research documents, whether they are published or not. The documents may come from teaching and research institutions in France or abroad, or from public or private research centers.

L'archive ouverte pluridisciplinaire **HAL**, est destinée au dépôt et à la diffusion de documents scientifiques de niveau recherche, publiés ou non, émanant des établissements d'enseignement et de recherche français ou étrangers, des laboratoires publics ou privés.

# Progress in calibration-free laser-induced breakdown spectroscopy

Jörg Hermann<sup>a,\*</sup>, Christoph Gerhard<sup>b</sup>, Miloš Burger<sup>c</sup>, Valentin Craciun<sup>d</sup>, Frédéric Pelascini<sup>e</sup>

<sup>a</sup>Aix-Marseille University, CNRS, LP3, 13288 Marseille, France

<sup>b</sup>University of Applied Sciences and Arts, Faculty of Engineering and Health, 37085 Göttingen, Germany

<sup>c</sup>University of Michigan, Gérard Mourou Center for Ultrafast Optical Science, Ann Arbor, MI 48109, USA

<sup>d</sup>National Institute for Laser, Plasma and Radiation Physics, 77125 Măgurele, Romania

<sup>e</sup>Cetim Grand Est, 67400 Illkirch-Graffenstaden, France

---

## Abstract

Direct elemental analysis of materials via modeling of the laser-produced plasma emission attracted great interest since the introduction of calibration-free laser-induced breakdown spectroscopy in 1999. However, the large number of different approaches and their validation in diverse experimental conditions make it difficult to evaluate the achievable performance with this revolutionary type of analytical measurements. The purpose of the present paper is to provide a critical review of the development of calibration-free LIBS, to highlight the progress being achieved until now, and to estimate its available analytical performance. Based on the identification of the principal sources of measurement uncertainty, solutions are proposed to further improve the accuracy in order to bring calibration-free LIBS to the standard of fully recognized analytical methods.

*Keywords:* LIBS; calibration-free; elemental analysis; measurement uncertainty; analytical performance; self-absorption; trace elements;

---

## 1. Introduction

The basic concept behind calibration-free laser-induced breakdown spectroscopy has been developed far before the invention of the laser. Plasma technologies emerged at the beginning of the last century [1], with principal objectives devoted to the understanding of astrophysical plasmas and to the investigation of the atomic structure. Later, the concept of local thermodynamic equilibrium (LTE) was introduced to enable a simplified description of the elementary processes that occur in a plasma [2]. Among them, we can distinguish collisional processes, such as excitation and ionisation by electron collisions and their inverse processes, and radiative processes, such as spontaneous emission and absorption between bound and free electronic states. Out of equilibrium, complex collisional-radiative modeling is required to describe the plasma, and the rates of all processes must be known [3].

In thermodynamic equilibrium, the principle of microscopic reversibility applies and each process is counterbalanced by its inverse process. A simplified

description of the plasma is thus possible via the statistical laws of equilibrium. So, the species velocities are described by the Maxwellian distribution, the excited-states population number densities are given by the Boltzmann law, the chemical and ionization equilibrium is described by Saha-equations, and the radiation equilibrium is governed by Planck's law [2].

The size of laboratory plasmas being typically smaller than the characteristic length of absorption, the principle of microscopic reversibility does not apply to radiative processes. The plasma may, however, reach the state of equilibrium, if the collisional processes dominate. In that case, the plasma is called in local thermodynamic equilibrium and described by all above mentioned equilibrium laws, except Planck's law [2].

In strongly ionized plasmas, the collisional processes are dominated by the electrons and the establishment of LTE requires thus a large enough electron density, above a minimum value that can be estimated using the criteria proposed by Griem [4], McWhirter [5], and Drawin [6]. In literature, most studies refer to the criterion of McWhirter due to the simplicity of its implementation.

To investigate the LTE state, appropriate plasma sources such as stabilized arcs [1], shock tubes [7] or

---

\*Corresponding author: jorg.hermann@cnrs.fr

spark discharges [8] have been developed. Operated at atmospheric pressure, the time of thermalization - that is the time required for the establishment of equilibrium - equals the characteristic times of particle and heat diffusion [9]. Plasmas in LTE are therefore spatially nonuniform and their diagnostics require space-resolved spectroscopic measurements and complex data analyses [10].

Laser-produced plasmas appeared later. Their early spectroscopic observations were mostly dedicated to the study of laser-matter interaction [11, 12] and to analytical measurements [13, 14]. Their use as a source for plasma spectroscopy was limited. Laser-produced plasmas have small sizes and are characterized by fast expansion dynamics. They had low reproducibility during the early experiments due to the poor stability of the available laser sources.

Technological advances changed the situation. Reliable gain-switched Nd:YAG laser sources, delivering pulses of nanosecond duration with high energy and pointing stabilities, enabled the generation of highly reproducible plasmas [15]. Fast and sensitive intensified charge-coupled detectors rendered the time- and space-resolved spectroscopic observation of the small-sized and rapidly expanding laser-induced plasmas accessible. The interest for LIBS increased, in particular during the last two decades, where an exponential increase of the number of publications related to the subject was observed [16]. The increase of interest was not only dedicated to analytical measurements but also to investigations of plasma fundamentals [17, 18, 19]. The laser-induced plume as a plasma source for measurements of spectroscopic data became popular [20, 21, 22, 23]. The small size appeared now as an advantage as it limits the amount of self-absorption.

Plumes produced by pulsed laser ablation are singular plasma sources. Compared to other atmospheric pressure plasmas, they are characterized by a much higher initial density, followed by fast expansion until a pressure equilibrium with the surrounding gas is reached [24]. The high density makes thermalization faster, and renders diffusion processes slower. Thus, plasmas produced by laser ablation are characterized by a time of thermalization smaller than the times of diffusion. They may therefore combine two properties which are generally not found together: the local thermodynamic equilibrium and the spatial uniformity. Both properties were found together for the plasma produced by ultraviolet nanosecond laser ablation under argon atmosphere [25]. They were evidenced by the simultaneous observation of three features in the plasma emission spectrum: (i) the emission spectrum

is accurately described by the spectral radiance of a uniform LTE plasma, computed by using an analytical solution of the radiation transfer equation. Thus, the most intense lines were found to saturate at the blackbody spectral radiance, and the blackbody temperature equaled the atomic excitation temperature deduced from the Boltzmann plot of optically thin lines [25, 26]. (ii) The observation of symmetric profiles of Stark-shifted spectral lines. Such lines appear asymmetric when emitted from a nonuniform plasma, like the vapor plume produced by laser ablation of a solid sample in air [25, 27]. (iii) The absence of absorption dips in the profiles of strongly self-absorbed resonance lines [25, 27].

The combination of both properties in the laser-induced plasma constitutes a breakthrough in the development of calibration-free LIBS as it enables, via robust and accurate modeling of the plasma emission spectrum, elemental analysis of materials with an accuracy not attainable before [28, 29]. Moreover, straightforward measurements of spectroscopic data, such as Einstein coefficients of spontaneous emission and Stark broadening parameters, become accessible without the need of space-resolved spectroscopic observations, simplifying thus this kind of measurements [22, 30]. This opens multiple perspectives for all applications requiring spectroscopic data, as the number of reliable data and their quality are expected to grow rapidly within the next years.

In the following, we briefly recall basic fundamentals of calibration-free LIBS, before presenting a short review of its development in Section 3. Then, the analytical performance will be critically analyzed in Section 4, and upcoming still required improvements will be discussed in Section 5.

## 2. Fundamentals

The simplest way to calculate the emission spectrum of a spatially uniform plasma is to approximate its shape by a layer of thickness  $L$  as shown in Fig. 1, in order to describe the radiation transfer as a one-dimensional problem. The intensity variation of the radiation flux propagating along the  $z'$ -axis towards the observer [see Fig. 1(c)] is given by

$$n(z') \frac{d}{dz'} \left( \frac{I_\lambda(z')}{n^2(z')} \right) = \varepsilon_\lambda(z') - \alpha(z') I_\lambda(z'), \quad (1)$$

where  $\varepsilon_\lambda$ ,  $\alpha$  and  $n$  are the emission coefficient, the absorption coefficient and the refractive index of the

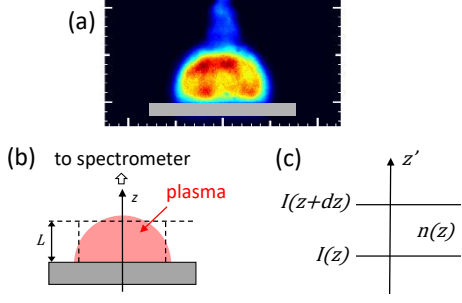


Figure 1: (a) Image of the plasma produced by UV laser ablation under argon atmosphere. Schematics illustrating (b) the geometry of spectroscopic observation and (c) the radiation flux propagating along the  $z'$ -axis in a medium of refractive index  $n$ .

medium, respectively. For a plasma, we have  $n \simeq 1$ . Assuming a spatially uniform medium, integration of Eq. (1) along the line of sight leads to

$$I_\lambda(z) = \frac{\varepsilon_\lambda}{\alpha} (1 - e^{-\alpha z}). \quad (2)$$

In local thermodynamic equilibrium, the coefficients of emission and absorption are related via Kirchhoff's law of thermal radiation to the blackbody spectral radiance

[31]

$$B_\lambda^0(\lambda) = \frac{\varepsilon_\lambda(\lambda)}{\alpha(\lambda)}, \quad (3)$$

and the spectral radiance of the uniform plasma in LTE is given by

$$B_\lambda(\lambda) = B_\lambda^0(\lambda) (1 - e^{-\tau(\lambda)}). \quad (4)$$

Here,  $\tau(\lambda) = \int \alpha(\lambda, z) dz = \alpha(\lambda)L$  is the optical thickness that accounts for the amount of self-absorption.

In the case of negligible self-absorption ( $\tau \ll 1$ ), Eq. (4) becomes

$$B_\lambda(\lambda) = \varepsilon_\lambda(\lambda)L. \quad (5)$$

The spectral radiance of the plasma, and thus the measured intensity, are proportional to the emission coefficient. In the opposite case of strong self-absorption ( $\tau \gg 1$ ), Eq. (4) simplifies to

$$B_\lambda(\lambda) = B_\lambda^0(\lambda). \quad (6)$$

Microscopic reversibility between the processes of emission and absorption applies in a given spectral range, a situation that is generally limited to strong resonance transitions and a narrow wavelength interval close to the line center wavelength.

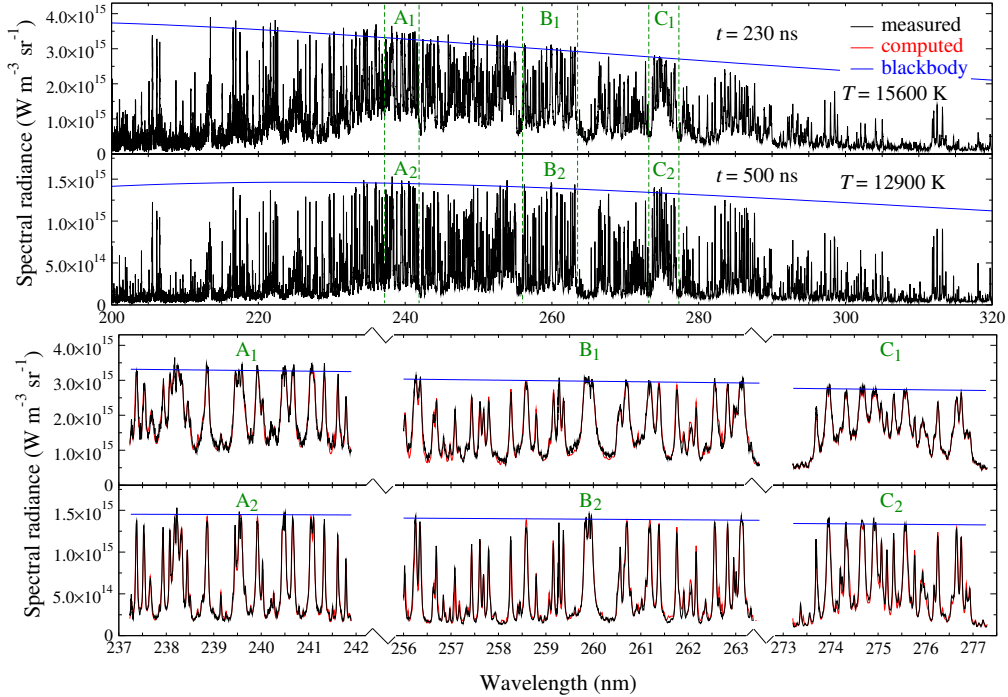


Figure 2: Space-integrated spectra recorded during laser ablation of steel in argon at different times. The strongest transitions are shown to saturate at the blackbody spectral radiance. The excellent agreement with the spectral radiance computed using Eq. (4) shows that the emission originates from a uniform plasma in LTE. (Adapted from Ref. [25])

### 2.1. Evidence of blackbody radiance

The saturation of most intense lines at the blackbody radiance is illustrated in Fig. 2, where LIBS spectra of steel, recorded for two different delays between the laser pulse and the detector gate, are presented. Numerous lines are shown to reach the blackbody spectral radiance that was calculated for the temperature deduced from the intensity distribution of atomic and ionic lines. For three spectral ranges, the measured spectrum is displayed together with the spectral radiance computed according to Eq. (4). The excellent agreement between measured and computed spectra supports the hypothesis of a uniform plasma in LTE.

### 2.2. Symmetric profile of Stark-shifted line

In strongly ionized laser-produced plasmas, the shape of the spectral lines is mostly determined by the Stark effect [32]. The lines are therefore broadened and shifted, and the Stark widths and shifts increase linearly with the electron density in the case of non-hydrogenated transitions [33]. For a given transition, the Stark shift is typically smaller than the Stark width, and ranges from 0 to 30% for most lines [34]. The space-integrated observation of a strongly Stark-shifted line delivers information about the spatial distribution of the electron density  $n_e$  within the plasma. In the case of a nonuniform plasma, typically characterized by a hot core and a cold border, the line profiles emitted from the plasma volumes of different  $n_e$ -values have unequal widths and shifts as illustrated in Fig. 3. The resulting line shape recorded by the spectroscopic apparatus is therefore asymmetric. In opposition, the observation of a symmetric shape of a strongly Stark-shifted line proves that the plasma has a uniform electron density distribution.

Measured profiles of a strongly Stark-shifted line are

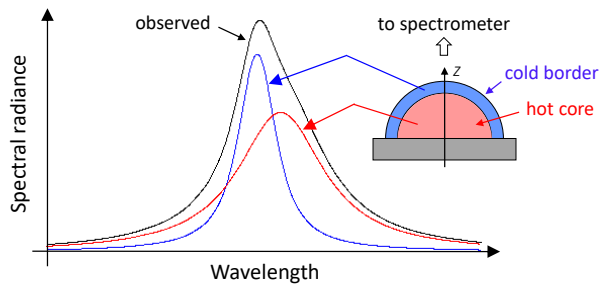


Figure 3: Illustration of the line shape of a strongly Stark-shifted transition emitted from a nonuniform plasma. The superposition of profiles with different widths and shifts results in an asymmetric line shape captured by the spectroscopic apparatus.

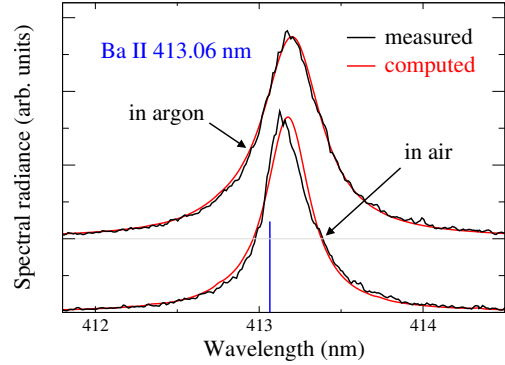


Figure 4: Ba II 413.06 nm line profile recorded during laser ablation of barite crown glass for  $t = 500$  ns. Comparison to the spectral radiance computed for a uniform LTE plasma. The blue line indicates the resonance wavelength of the transition. (Adapted from Ref. [25])

displayed in Fig. 4. They were recorded during ultra-violet laser ablation of optical glass in ambient air and argon background gas. The comparison with computed symmetric line shapes shows that the line profile observed for ablation in air is asymmetric, indicating thus a nonuniform  $n_e$ -distribution. In opposition, the line profile observed for ablation in argon appears symmetric, showing thus that the plume generated in the inert gas has a uniform electron density distribution.

The observed difference illustrates the influence of the background gas on the properties of the ablated vapor plume. For a molecular gas such as air, the interaction at the vapor-gas contact front is dominated by inelastic collisions, due to the numerous rovibrational levels of the gas molecules. This leads to efficient cooling of the peripheral volume of the vapor plume. In an inert gas such as argon, most collisions are elastic due to the high energy required for excitation (11.55 eV for Ar). The electrons conserve most of their energy, and the surrounding gas acts like an isolating layer.

### 2.3. Absorption dip of resonance line

In a nonuniform plasma, the values of temperature and electron density are typically lower in the peripheral volume compared to their values in the plasma core. The population number densities of ground state species are therefore large, and the resonance lines undergo strong absorption in the border volume. According to the reduced electron density, the strongly broadened line emitted from the core volume, is reabsorbed in a narrow spectral range, close to the resonance wavelength of the transition (see Fig. 5). The resulting spectral line shape is thus characterized by an absorption dip that illustrates the occurrence

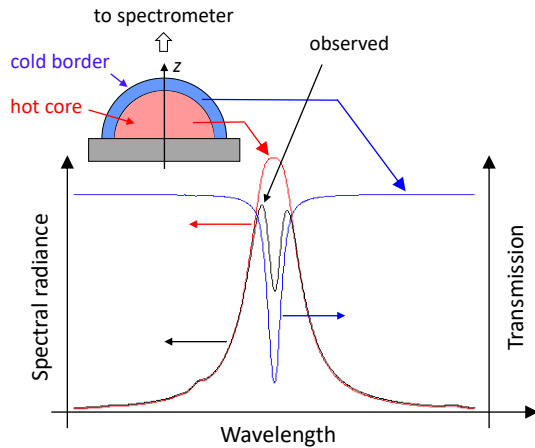


Figure 5: Illustration of the line shape of a strongly self-absorbed resonance line emitted from a nonuniform plasma. The large line profile emitted from the hot core is reabsorbed by the cold border in a narrow spectral range close to the resonance wavelength, according to the reduced electron density. The observed line shape exhibits thus an absorption dip.

of nonuniform distributions of electron density and temperature [35, 36].

Measured profiles of a resonance line are displayed in Fig. 6. They were recorded during ultraviolet laser ablation of pure indium in ambient air and argon background gas. The line observed in air exhibits an absorption dip that confirms the nonuniform plasma distribution deduced from the observation of a strongly Stark-shifted transition (see Section 2.2). In opposition, the absorption dip is not observed for line emission in argon. This confirms the results presented in Figs. 2 and 4, showing that the vapor plume produced by

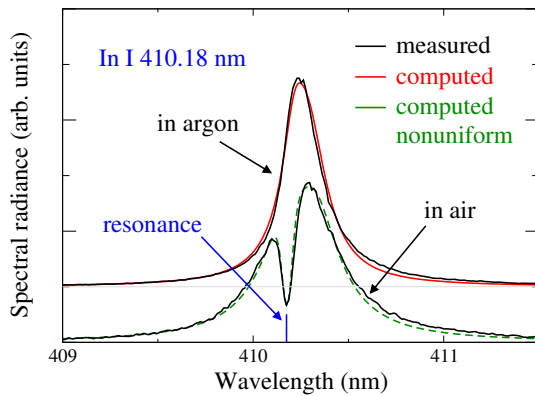


Figure 6: In I 410.18 nm resonance line recorded during laser ablation of indium for  $t = 500$  ns. The measurements in argon and air are compared to the spectral radiances of a uniform and a nonuniform LTE plasma, respectively. (Adapted from Ref. [25])

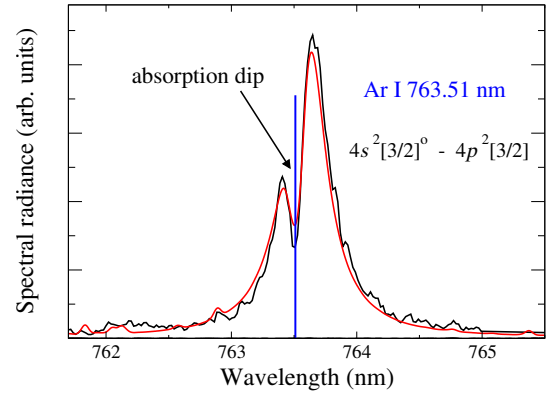


Figure 7: Measured (black line) and computed (red line) shapes of an Ar transition toward the metastable state. The recording was performed during ablation of steel in argon for  $t = 500$  ns. The simulation was obtained by adding two layers to the laser plasma, representing the heated gas at the vapor-gas contact front and the adjacent colder gas. The absorption dip was observed for each investigated material.

ultraviolet laser ablation in argon has almost uniform distributions of temperature and electron density.

The uniform spatial distributions observed in argon are however restricted to the vapor plume, and gradients of temperature and electron density are naturally expected in the surrounding background gas, to provide the transition from the heated gas layer at the vapor-gas contact front towards the cold environment.

The presence of temperature and electron density gradients in the argon background gas is illustrated by the absorption dip in the profile of the argon line displayed in Fig. 7. The Ar I 763.51 nm transition decays towards a metastable state. According to the large energy gap of 11.55 eV towards the ground state, the collisional desexcitation is slow, and the metastable state is expected to reach a large population number density. The spectral line behaves therefore like a resonance transition, characterized by strong self-absorption that enables here the visualization of gradients in the background gas.

### 3. Development of calibration-free LIBS

#### 3.1. Successful introduction of first method

The development of calibration-free laser-induced breakdown spectroscopy started in 1999 with the approach of Ciucci et al. [37]. The method was based on the hypotheses that (i) the mass transfer from the solid into the plasma is congruent, (ii) the plasma is in local thermodynamic equilibrium, (iii) the plasma has spatially uniform distributions of temperature and

densities, and (iv) self-absorption of spectral lines is negligible. In that case, the measured line intensity is proportional to the emission coefficient [see Eq. (5)]. Assuming furthermore moderate ionisation, the elemental fractions can be directly deduced from the multielemental Boltzmann plot.

This method attracted great interest due to the simplicity of its implementation [38]. Applied by many research groups on all kind of materials, the analytical performance was however found to be limited [39]. The low performance was due to the fact that the hypotheses of model validity were generally not all satisfied. Although it is now well accepted that experimental conditions can be easily found to satisfy the hypotheses of congruent ablation [40, 41] and LTE [42, 43], and that spatial uniformity can be reached in appropriate experimental conditions (see Section 2), the condition of optically thin emission is hardly achieved for dense laser-induced plasmas [36, 44, 45].

### 3.2. Amended methods

Amendments have thus been proposed, most of them dedicated to the compensation of self-absorption [46, 47, 48]. Later, approaches based on the spectra simulation have been developed [49, 50, 51]. These have the advantage that they intrinsically account for self-absorption.

However, compared to the initial calibration-free LIBS method proposed by Ciucci et al. [37], the amended approaches were associated to a significant increase of complexity in their implementation. Their use was therefore restricted to a limited number of research groups, and numerous authors reported calibration-free LIBS analysis by carefully selecting optically thin spectral lines [52, 53].

As absorption and emission are correlated in LTE plasmas according to Kirchhoff's law of thermal radiation [see Eq. (3)], the selection of optically thin lines implies the restriction to transitions of weak intensity, lowering thus the analytical performance via the reduced signal-to-noise ratio.

More recently, methods including a single calibration step have been introduced to improve the accuracy of the analytical measurement [54, 55, 56]. Here, the spectrum measured for a single standard sample is used to compensate errors due to the apparatus response function and spectroscopic data. This improvement is however limited, as the spectroscopic data - that are transition probabilities and Stark broadening parameters - impact the amount of self-absorption [57], whereas the apparatus response has a linear influence

on the measured line intensity [58]. Consequently, the accuracy improvement due to the single calibration step works properly only when optically thin lines are used, or when the elemental fractions to be measured are close to those of the standard sample.

### 3.3. General remarks

The rich literature dedicated to the development of calibration-free LIBS analysis and its validation in a large variety of different experimental conditions makes it difficult to choose the appropriate method for a particular compositional measurement and to predict the achievable analytical performance. Thus, before discussing accuracy and current limitations, we would like to make several general comments on both the development of calibration-free LIBS and its validation:

(i) Most of the proposed calibration-free LIBS approaches are based on the same physical model: the spatially uniform LTE plasma. They are therefore expected to have similar analytical performance.

(ii) Methods based on spectra simulation and methods based on the multielemental Boltzmann plot are often considered as fundamentally different approaches, with distinguished pathways for obtaining the fundamental parameters that describe the plasma. Furthermore, spectra simulation is often associated to time-consuming calculations. The reason for this is that some authors combined spectra simulation with Monte-Carlo calculations to find the plasma parameters [59, 60]. This is however not required for the simple case of the uniform LTE plasma for which the parameters can be found straightforwardly [43].

Moreover, the number of parameters is independent of the kind of approach and depends uniquely on the physical model. When the spectrum is computed via the analytical solution of the radiation transfer equation given by Eq. (4), the calculation is fast and no significant difference is expected in the computational duration of spectra-simulation-based calibration-free LIBS compared to the analysis through the multielemental Boltzmann plot. The fundamental difference relies in the data processing methodology only: in the case of the multielemental Boltzmann plot, the analysis starts with the experimental spectrum via measurements of line intensities and widths. Contrarily, in spectra simulation, the starting point is the calculation of the plasma emission spectrum that is then compared to the measured one.

Methods based on spectra simulation facilitate automation of calibration-free LIBS analysis as the treatment

of line interferences is much easier to handle.

(iii) The validation of the calibration-free LIBS methods is exclusively done by comparing the final result of the elemental analysis with the reference composition [61, 62, 63]. This makes it difficult to identify individual error sources, and thus to predict the analytical performance for a given type of material.

## 4. Analytical performance

### 4.1. Accuracy of minor or trace element quantification

#### 4.1.1. Influence of closure condition on accuracy

Calibration-free LIBS is generally considered to have low accuracy in minor and trace element quantification [38]. This is often attributed to the closure condition according to which the sum over all elemental fractions equals unity ( $\sum_A C_A = 1$ ) [39, 64]. It is thus expected that even small errors of major element fractions induce large errors to minor and trace element fractions.

The mass fraction of an element  $A$  is given by  $C_A = n_A m_A / \rho_{tot}$ , where  $n_A$  and  $m_A$  are the atomic number density and the atomic mass of element  $A$ , respectively, and  $\rho_{tot} = \sum_A n_A m_A$  the specific mass of the plasma. Applying the partial derivations with respect to the atomic number densities of all sample-composing elements, we obtain the uncertainty associated to the fraction measurement

$$\frac{\Delta C_A}{C_A} = \sqrt{(1 - C_A)^2 \left(\frac{\Delta n_A}{n_A}\right)^2 + \sum_{j \neq A}^N C_j^2 \left(\frac{\Delta n_j}{n_j}\right)^2}. \quad (7)$$

The factor  $(1 - C_A)^2$  in the first term of the quadratic sum illustrates that elements of large abundance have reduced fraction measurement uncertainties. Contrarily, elements of small abundance are characterized by a measurement uncertainty that has significant contributions from the major elements as indicated by the sum of the quadratic errors weighted by the  $C_j^2$ -values.

For clear illustration, we consider a sample composed of only two elements, a major and a trace element. Neglecting self-absorption and ignoring all error sources except the intensity measurement error, that is supposed to be equal for both elements, Eq. (7) simplifies to

$$\frac{\Delta C_A}{C_A} = \sqrt{(1 - C_A)^2 \left(\frac{\Delta I}{I}\right)^2 + C_B^2 \left(\frac{\Delta I}{I}\right)^2}. \quad (8)$$

For a major element ( $C_A \rightarrow 1$ ) and a trace element ( $C_B \rightarrow 0$ ), the uncertainties become  $\Delta C_A / C_A \rightarrow 0$  and  $\Delta C_B / C_B \rightarrow \sqrt{2} \Delta I / I$ , respectively. The closure

condition leads thus to a reduction of the fraction measurement uncertainty of major elements and a moderate uncertainty increase for minor and trace elements.

#### 4.1.2. Influence of LTE condition on accuracy

Calibration-free LIBS requires emission spectra recorded in experimental conditions for which the plasma is in local thermodynamic equilibrium. The equilibrium state is established when the electron density is large enough to satisfy the LTE criteria (see Section 1). The large number density of charged particles is associated to intense continuum emission due to bremsstrahlung and radiative recombination.

As  $n_e$  decreases in time, spectra used for calibration-free LIBS measurements have to be recorded with a short enough detector gate delay, as illustrated in Fig. 8. In calibrated LIBS, there is no need of LTE and a larger gate delay is generally applied to achieve best signal-to-noise ratio. The need of LTE leads thus to lowering of the signal-to-noise ratio in calibration-free LIBS measurements. Consequently, the measurement accuracy is reduced for analytical lines of low emission intensity that generally belong to minor or trace elements.

The lowering of accuracy is particularly severe if the sample composition contains major elements with large energy gaps in their atomic structure, such as C, H, N or O [43]. In that case, a larger electron density is required to establish LTE, and spectra recording at shorter delay leads to further reduction of the signal-to-noise ratio. The loss of sensitivity is thus amplified in calibration-free LIBS analyses of glass [29] or organic materials such as food [65].

To improve the sensitivity of calibration-free LIBS analysis of such materials, a two-step method was proposed [65]. It consists of recording two spectra with

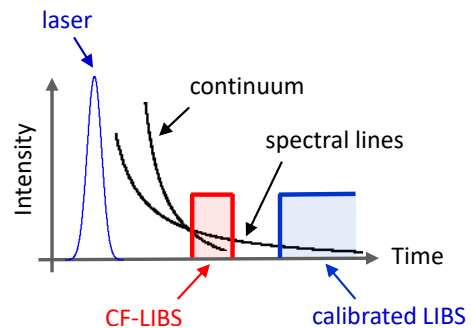


Figure 8: Schematic illustrating the setting of detector gate delay and width for spectra recording in calibration-free and calibrated LIBS.

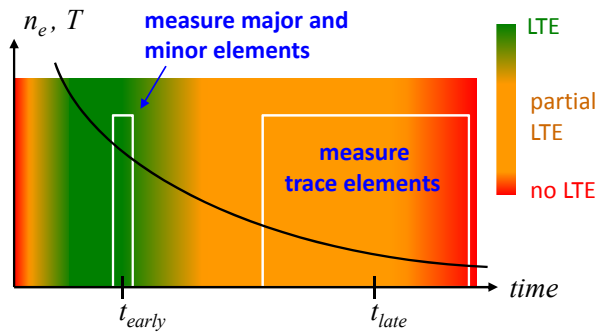


Figure 9: Time scheme of two-step procedure for sensitivity-enhanced calibration-free LIBS: two spectra are recorded at different times. The early recording in conditions of full LTE serves to quantify major and minor elements. The late recording in conditions of partial LTE serves to measure minor and trace elements. The color scale from green to red indicates the degree of equilibrium. (Adapted from Ref. [65])

different delays between the laser pulse and the detector gate as illustrated in Fig. 9. The early measurement is performed with a delay sufficiently short, so that the electron density is large enough to ensure full LTE conditions. Here, the signal-to-noise ratio is high enough to enable the quantification of elements having large abundance, but too small for fraction measurements of trace elements.

The late measurement is therefore performed in conditions of partial LTE, for which matrix elements with large energy gaps in their atomic structure are out of equilibrium, whereas atoms and ions of all other elements have Boltzmann equilibrium distributions. According to the reduced electron density, the signal-to-noise ratio is increased, and trace elements can be quantified. The combination of both measurements enables thus the analysis of the entire sample composition, as demonstrated for glass [43] and seafood [65].

#### 4.1.3. Influence of probe volume on accuracy

Another error source of calibration-free LIBS measurements can be attributed to the probe volume, that generally differs from that of the reference method. As the fractions of trace elements on the sample surface often differ from their values in the bulk material, the measured value is probe volume-dependent.

To account for possible nonuniform elemental distributions, in-depth measurements can be performed by recording spectra for laser pulses applied successively to the same irradiations sites [66]. Such measurements are of particular interest in combination with calibration-free spectra analysis, as possible changes of electron density and temperature within the plasma

produced by successive laser pulses are taken into account [41].

The fractions of trace elements as functions of depth measured via depth-resolved calibration-free LIBS are displayed in Fig. 10 for analysis of optical glass. Three types of trace elements can be distinguished: elements that belong to the glass matrix having a depth-independent mass fraction (a); elements originating from the polishing agent, characterized by an exponential decrease over a few micrometers towards zero (b); and elements with contributions from both the polishing solution and the glass matrix, characterized thus by an exponential decrease towards a constant value (c).

Comparing the mass fractions deduced for the bulk to reference values measured via inductively-coupled plasma atomic emission spectrometry, a good agreement was found for the entire glass composition including major, minor and trace elements [29].

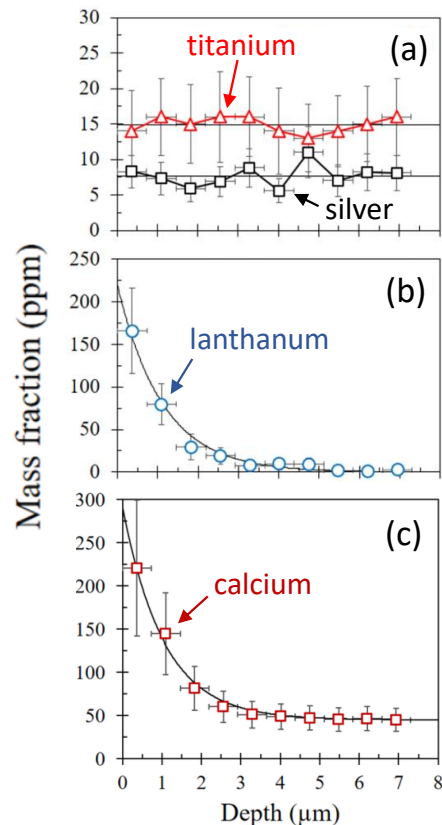


Figure 10: Trace element fractions of heavy flint glass (Schott, SF5) versus depth measured via depth-resolved calibration-free LIBS. (Adapted from Ref. [29])

In summary, compared to the analytical performance of calibrated LIBS, the measurement accuracy of calibration-free LIBS analysis is reduced for minor and trace elements. However, the accuracy lowering is moderate if the measurements were performed in appropriate experimental conditions (see Sections 4.1.2 and 4.1.3).

#### 4.2. Accuracy lowering due to self-absorption

Numerous approaches have been proposed to account for self-absorption in calibration-free LIBS [46, 47, 48]. Some authors reported methods that enable the use of even strongly self-absorbed transitions, having an optical thickness up to  $10^2$  [64, 67]. Recently, a method was proposed to compensate self-absorption via the exploitation of blackbody radiation [68]. All these methods have been proposed without the evaluation of the analytical measurement uncertainty that is expected to grow according to the decrease of the slope of the curve of growth with increasing optical thickness (see Fig. 11). The quantification of the measurement uncertainty due to self-absorption is however essential for choosing the most appropriate spectral lines, and consequently for the optimizing the analytical performance.

To quantify the increase of analytical measurement uncertainty due to self-absorption, the uncertainty of the atomic number density  $\Delta n_A$  in Eq. (7) must be evaluated. Neglecting the uncertainties of temperature and electron density, we obtain in case of optically thin ( $\tau \ll 1$ ) emission [57]

$$\frac{\Delta n_A}{n_A} = \sqrt{\left(\frac{\Delta I}{I}\right)^2 + \left(\frac{\Delta A_{ul}}{A_{ul}}\right)^2}, \quad (9)$$

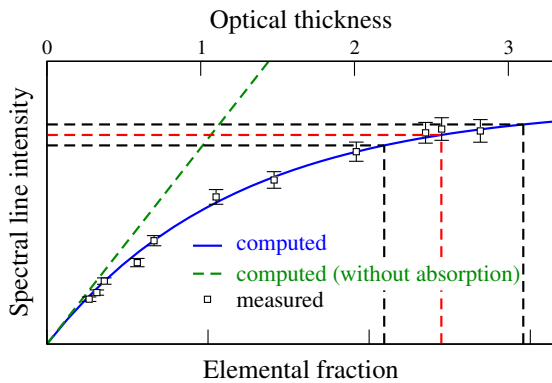


Figure 11: Curve of growth of a self-absorbed transition. The spectral line intensity measured for various elemental fractions is compared to the intensity computed according to Eq. (4). (Adapted from Ref. [57])

where  $\Delta I$  and  $\Delta A_{ul}$  are the uncertainties of the measured line intensity and the transition probability, respectively. The uncertainty  $\Delta I$  accounts for line interferences, signal-to-noise ratio, and the uncertainty of the apparatus response function.

In the general case, when self-absorption reduces the emission intensity of the spectral line, the analytical measurement uncertainty is given by [57]

$$\frac{\Delta n_A}{n_A} = \sqrt{\left(\frac{\Delta \tau_0}{\tau_0}\right)^2 + \left(\frac{\Delta A_{ul}}{A_{ul}}\right)^2 + (1 - e^{-\tau_0}) \left[ \left(\frac{\Delta w_{sd}}{w_{sd}}\right)^2 + \left(\frac{\Delta L}{L}\right)^2 \right]}. \quad (10)$$

Here,  $\Delta \tau_0$  is the uncertainty of the line center optical thickness that accounts for the increase of analytical measurement uncertainty due to the reduction of the slope of the curve of growth (see Fig. 11). The spectral line width due to Stark and Doppler broadening  $w_{sd}$  and the plasma size along the line of sight  $L$  determine the amount of optical thickness, and the associated uncertainties  $\Delta w_{sd}$  and  $\Delta L$  determine thus the uncertainty of horizontal scaling of the curve of growth.

##### 4.2.1. Accuracy lowering due to the reduction of the slope of the curve of growth

The uncertainty  $\Delta \tau_0$  can be expressed as a function of the intensity measurement uncertainty via

$$\frac{\Delta \tau_0}{\tau_0} = g(\tau_0) \frac{\Delta I}{I}, \quad (11)$$

where the error growth factor  $g(\tau_0)$  is obtained from the  $I = f(\tau_0)$  dependence that can be calculated using Eq. (4). For center of line intensity measurements, the error growth factor in case of negligible apparatus spectral broadening has an analytical expression given by [57]

$$g_0 = \frac{1 - e^{-\tau_0}}{\tau_0 e^{-\tau_0}}. \quad (12)$$

It describes the exponential error growth that is expected from the saturation of the center of line intensity at the blackbody radiance level [see Eq. (6)].

For measurements of the line-integrated intensity, no analytical expression  $I_{line} = f(\tau_0)$  exists for common line shapes represented by the Voigt profile, and  $g(\tau_0)$  must be computed numerically. For most common transitions having a significant contribution of Stark broadening, a moderate error growth  $g \leq 2$  is expected according to the square root dependence of the curve of growth for  $\tau_0 \gg 1$  [69].

#### 4.2.2. Accuracy lowering due to line width uncertainty

The line width due to Stark and Doppler broadening determines the amount of self-absorption, and its uncertainty has an influence on the analytical measurement uncertainty that increases with the optical thickness according to Eq. (10). The Doppler width is typically of about a few picometers, and therefore much smaller than the apparatus spectral width  $w_{app}$  of most LIBS systems. The accuracy of the line width  $\Delta w_{sd}$  depends thus on the ratio between Stark width  $w_s$  and apparatus width [57]. For strongly Stark-broadened lines, when  $w_s \geq w_{app}$ , the line width can be measured. In that case, an accuracy of  $\Delta w_{sd} \approx 5\%$  can be reached. In the opposite case of weakly Stark-broadened lines, when  $w_s < w_{app}$ , the line width cannot be accurately measured. It is therefore computed, and  $\Delta w_{sd}$  is large due to the elevated uncertainties associated to the electron density and the Stark broadening parameter of most transitions [70]. A typical value  $\Delta w_{sd} \geq 25\%$  is expected in that case.

#### 4.2.3. Accuracy lowering due to the uncertainty of plasma size

The plasma size can be deduced from the intensity ratio of spectral lines having significantly different optical thicknesses [43] or from fast plasma imaging [71]. In both cases, the uncertainty of the plasma size is large, and a value of  $\Delta L \approx 10\%$  is expected in the best case.

In summary, self-absorption lowers the accuracy of the analytical measurement. The loss of accuracy may be moderate if the line width  $w_{sd}$  and the plasma size  $L$  are precisely known. For resonance lines,  $w_{sd}$  is often small and therefore deduced from calculation. In that case,  $\Delta w_{sd}$  is generally large and the loss of accuracy due to self-absorption is high.

#### 4.3. Other sources of uncertainty

The uncertainties associated with plasma temperature, electron density, and the failure of model validity are ignored in the evaluation of the analytical performance by means of Eq. (10). The failure of model validity can be avoided by choosing the appropriate experimental conditions (see Section 2). Temperature and electron density are secondary error sources, as  $\Delta T$  and  $\Delta n_e$  are resulting from the uncertainties associated with spectroscopic data and experimental parameters [72]. Aside from the accuracy improvement related to the primary error sources,  $\Delta T$  and  $\Delta n_e$  can be minimized statistically by deducing average values from a large number of measured lines. Thus, their influence on the analytical measurement uncertainty is expected to be small compared to the direct influence of the primary error sources expressed in Eq. (10).

### 5. Upcoming improvements

Although calibration-free laser-induced breakdown spectroscopy has been shown to enable accurate analyt-

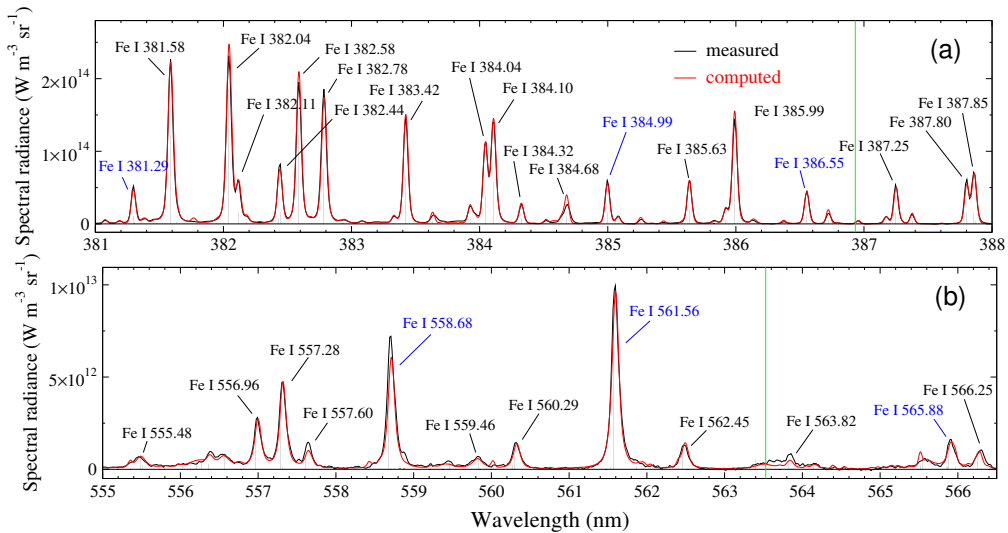


Figure 12: Measured and computed spectra of steel displayed for spectral windows in the blue (a) and the green (b) ranges. The blue-labelled transitions were selected to deduce the ratio between measured and computed intensities. (Adapted from Ref. [58])

ical measurements when it is performed in appropriate experimental conditions [28, 29, 30], there are still obstacles that hinder its use in industrial applications.

### 5.1. Compensation of the apparatus response

To compare the measured spectrum to emission of a plasma in LTE, the intensity of the recorded spectrum must be corrected by the apparatus response function. The apparatus response is generally measured with radiation standards such as a deuterium arc and a tungsten filament lamp for the ultraviolet and visible/near infrared spectral ranges, respectively. The frequency of such measurements depends on the mechanical stability of the optical system.

Calibration-free LIBS is mostly operated with echelle spectrometers to record broadband spectra in which lines of all sample-composing elements can be observed. Echelle spectrometers exploit dispersion of light into two orthogonal directions, and both their spectral and intensity calibration are therefore sensitive to temperature variation [73]. Thus, a method for rapid checking and correcting the apparatus response  $R_{app}(\lambda)$  was proposed [58].

#### 5.1.1. Checking $R_{app}(\lambda)$ using LIBS emission

The method is based on the simulation of the emission spectrum of a plasma produced by laser ablation of steel as shown in Fig. 12. Reliable transition probabilities are available for numerous lines of atomic and ionic iron [74], and the ratio between measured and computed line intensities can be used to verify the apparatus response as shown in Fig. 13 for hundreds of transitions, distributed all over the recorded emission spectrum. Here, the experimental conditions for the generation of a uniform LTE plasma (see Section 2) are exploited to enable the most accurate simulation of the plasma emission spectrum.

When the apparatus response of the measured spectrum was properly compensated, the ratio between measured and computed line intensities is a fluctuating function with an average value equal to unity all over the measured spectral range [see Fig. 13(a)]. In the opposite case, the average value of the intensity ratio varies as a function of wavelength as shown in Fig. 13(b). The wavelength-dependent change of the apparatus response is obtained by dividing the intensity ratio of the uncalibrated apparatus by that of the calibrated one (c). The approximation of the apparatus response change by a cosine-type function is then used to correct the apparatus response (d).

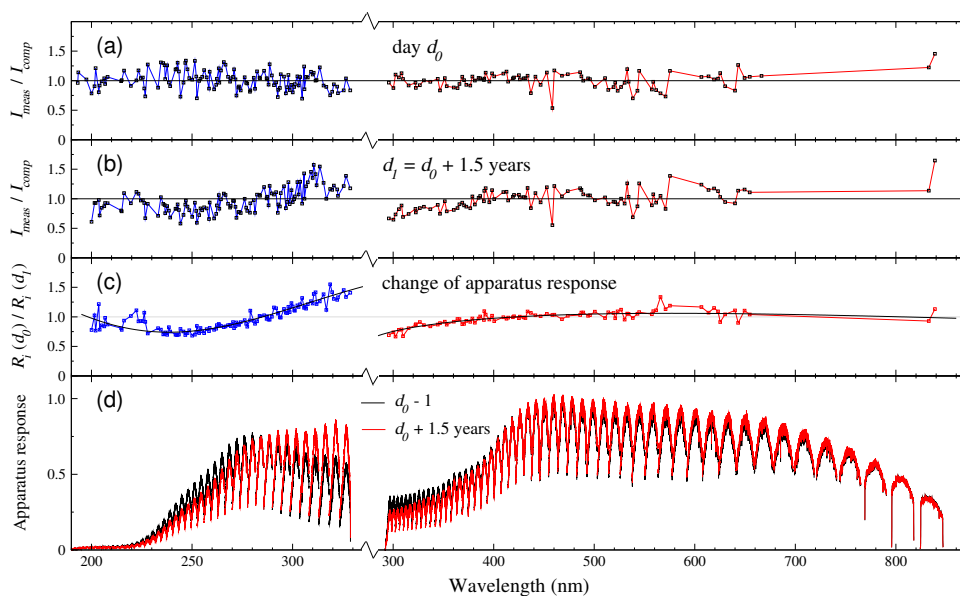


Figure 13: Ratio between measured and computed intensities  $R_i = I_{meas}/I_{comp}$  of spectral lines for spectra recordings (a) directly after the intensity calibration with radiation standards (day  $d_0$ ), and (b) 18 months later (day  $d_1$ ). (c) Change of apparatus response obtained by dividing the later  $R_i$ -value by the previous one. (d) Apparatus response measured on day  $d_0 - 1$  with calibration standards (black lines) and corrected apparatus response obtained for day  $d_1$ . The measurements were performed for UV and VIS/NIR ranges of an echelle spectrometer (LTB: model *Aryelle Butterfly*). (Adapted from Ref. [58])

### 5.1.2. Need of laser-plasma-based radiation standard

Although the method for rapid checking and correcting the apparatus response presents a progress in calibration-free LIBS, it still requires an initial measurement of  $R_{app}(\lambda)$  with classical radiation standards. The problem with these sources is that their emission spectra should be measured using the same optical path as the one used for the LIBS spectra recording. This is generally difficult or even impossible, in particular when commercial LIBS systems are used. Other drawbacks of classical radiation standards are the limited lifetime, typically of about 50 hours of use or 2 years of storage, and the high costs of their acquisition and calibration. The difficulty associated to the measurement of the apparatus response function presents therefore a major drawback that hinders the industrial development of calibration-free LIBS. To overcome this technological issue, the ideal solution would be to use the laser-induced plasma itself as a radiation standard. This could be achieved by exploiting the continuum radiation that dominates the plasma emission during the early stage of plume expansion. The operator would then be able to measure the apparatus response by simply changing the sample material and setting the appropriate delay of the gated detector.

### 5.1.3. Need of $T$ -stabilized echelle spectrometer

Echelle spectrometers are extremely sensitive to temperature variation and even small changes of the order of 1 K may alter the spectral calibration and the apparatus response function [73]. The loss of calibration may even occur when the spectroscopic apparatus is located in a temperature-stabilized laboratory environment, because the heat generated by the detector may cause temperature variation of the optical system [58]. Calibration-free LIBS measurements should therefore be performed with  $T$ -stabilized echelle spectrometers to ensure highest accuracy.

## 5.2. Need of accurate spectroscopic data

The analytical performance of calibration-free LIBS measurements depends on the quality of the available spectroscopic data. According to Eq. (10), accurate Einstein coefficients of spontaneous emission are required for all lines, and Stark broadening parameters must be accurately known for transitions for which self-absorption is significant.

Table 1: Wavelength  $\lambda$ , transition probability  $A_{ul}$  with accuracy  $\Delta A_{ul}$  (B+ := 10%; C := 25%; D := 40%), energies  $E$  of lower (index  $l$ ) and upper (index  $u$ ) levels of the most intense transitions of calcium atoms and ions according to NIST [74].

	$\lambda$ (nm)	$A_{ul}$ ( $\mu\text{s}^{-1}$ )	$\Delta A_{ul}$	$E_l$ ( $\text{cm}^{-1}$ )	$E_u$ ( $\text{cm}^{-1}$ )
Ca II	315.883	310	C	25 191.51	56 839.25
Ca II	317.933	360	C	25 414.40	56 858.46
Ca II	318.127	58	C	25 414.40	56 839.25
Ca II	370.602	88	C	25 191.51	52 166.93
Ca II	373.690	170	C	25 414.40	52 166.93
Ca II	393.366	147	C	0.00	25 414.40
Ca II	396.846	140	C	0.00	25 191.51
Ca II	409.709	9.9	D	60 533.02	84 933.65
Ca II	410.981	12	D	60 611.28	84 936.41
Ca II	422.007	8.5	D	60 611.28	84 300.89
Ca I	422.672	218	B+	0.00	23 652.304
Ca II	500.147	20	D	60 533.02	80 521.53
Ca II	501.997	23	D	60 611.28	80 526.16
Ca II	528.526	7.8	D	60 533.02	79 448.28
Ca II	530.722	15	D	60 611.28	79 448.28

### 5.2.1. Available spectroscopic data

**Transition probabilities.** The Einstein coefficients of spontaneous emission are tabulated in several atomic spectral line databases. Among them, the most complete lists of  $A_{ul}$ -values are given by the databases NIST [74] and Kurucz [75]. The NIST database is regularly updated. Compared to the Kurucz database, less but more reliable data are tabulated by NIST. Thus,  $A_{ul}$ -values are given by NIST for many transitions with their estimated accuracy. The data tabulated by Kurucz have been obtained by atomic structure calculations for which the evaluation of uncertainty is difficult. The  $A_{ul}$ -values are therefore given without any uncertainty interval.

Accurate Einstein coefficients are missing for many transitions and for many elements. As an example, the  $A_{ul}$ -values of the most intense lines of atomic and ionic calcium are listed in Table 1. Except the resonance transition of neutral calcium, the transition probabilities of lines are reported with an accuracy of 25% or 40%. The situation is similar for many other elements. More accurate data are tabulated for a few elements only. Iron is one of these elements, and the method for checking and correcting the apparatus response (see Section 5.1.1) was therefore implemented with Fe and Fe<sup>+</sup> transitions.

**Stark broadening parameters.** Stark broadening parameters of many transitions have been tabulated in the book of Griem [33] and in multiple review papers by Konjević and collaborators [34, 70, 76, 77, 78]. The accuracy of these data is low for most transitions, and estimated to about 20% to 30% in the best case. Data of

higher quality can be found for a few spectral lines only. Among them, the hydrogen Balmer alpha transition enables electron density measurements with 10% accuracy in typical conditions of LIBS experiments, where the electron density is of the order of  $1 \times 10^{17} \text{ cm}^{-3}$  [79, 80]. The temperature dependence is reported for a few transitions only [21, 80, 81]. For most transitions, the Stark broadening parameters are reported for given temperature values [34, 70, 76, 77, 78].

### 5.2.2. Imminent progress of spectroscopic database

The amount and the quality of spectroscopic data are continuously increasing as shown by the regular updates of the NIST database [74]. Here, measurements using the laser-induced plasma constitute a rising contribution over the past years [20, 21, 82]. The unique properties of the laser-produced plasma, that under appropriate experimental conditions combines spatial uniformity with local thermodynamic equilibrium (see Section 2), open new perspectives in the completion of spectroscopic databases. Accurate measurements of transition probabilities and Stark broadening parameters are thus possible, without the requirement of space-resolved spectroscopic observations and complex data analysis that are necessary with other LTE plasma sources [9, 10]. Thus, simple space-integrated observations with echelle spectrometers can be used to measure accurately spectroscopic data of numerous transitions at the same time [22, 30].

The potential of such measurements is illustrated by the fluctuation of the intensity ratio between measured and computed lines observed in Fig. 13. Indeed, the standard variation of this fluctuation equals the average uncertainty of the transition probabilities ( $\Delta A_{ul}/A_{ul} = 10\% \dots 15\%$ ). This indicates that  $A_{ul}$ -values can be measured with an expected accuracy of 5% or even better.

## 6. Conclusion

Calibration-free laser-induced breakdown spectroscopy is a powerful analytical tool, when operated in appropriate experimental conditions. It enables quantitative elemental analyses of the entire material composition, including major, minor and trace elements. The often reported reduced accuracy for the quantification of low-concentration elements is mostly attributed to the LTE condition and the probe volume. Solutions to limit the loss of analytical performance due to both effects are given by a two-step method and

indepth measurements presented in Sections 4.1.2 and 4.1.3.

Accuracy lowering due to self-absorption depends critically on the knowledge of the line width. Most resonance transitions have line widths smaller than the apparatus spectral width. The line width can be assessed by calculation only, which has low accuracy due to the large uncertainties of Stark broadening parameters and electron density. In that case, the loss of analytical performance due to self-absorption is significant.

The principal limitations that still hinder the use of calibration-free LIBS in industrial applications are related to the lack of accurate spectroscopic data and to the uncertainty of the apparatus response function. The further development of calibration-free LIBS analyses depends thus on the solutions to reduce the uncertainties associated to both error sources.

Concerning the spectroscopic data, frequent improvements can be observed in literature and by the regular updates of the NIST database, with an increasing contribution of measurements using the plasma produced by laser ablation. The unique properties of the laser-produced plasma, that may combine spatial uniformity with the LTE state, facilitate such measurements, and an acceleration in the progress of spectroscopic databases is expected.

To reduce the uncertainty of the apparatus response function, the use of temperature-stabilized echelle spectrometers is mandatory. Moreover, to overcome the difficulties associated to the measurement of the apparatus response with radiational standards, the development of a radiation standard based on the laser-induced plasma itself would remove the main obstacle that hinders the dissemination of compositional analysis via calibration-free laser-induced breakdown spectroscopy.

## 7. Acknowledgements

The research leading to these results has received funding from European Union's Horizon 2020 research and innovation programme under grant agreement No. 284464 and 654148 Laserlab-Europe (projects CNRS-LP3 002148, 002491 and 002585).

## References

- [1] A. G. Shenstone, Low voltage arc spectra of copper, *Nature* 114 (1924) 934–934.
- [2] H. R. Griem, *Plasma spectroscopy*, Academic, New York, 1964.
- [3] M. Capitelli, I. Armenise, D. Bruno, M. Cacciatore, R. Ce-liberto, G. Colonna, O. D. Pascale, P. Diomede, F. Esposito, C. Gorse, K. Hassouni, A. Laricchiuta, S. Longo, D. Pagano,

- D. Pietanza, M. Rutigliano, Non-equilibrium plasma kinetics: a state-to-state approach, *Plasma Sources Sci. Technol.* 16 (2007) S30–S44.
- [4] H. R. Griem, Validity of local thermal equilibrium in plasma spectroscopy, *Phys. Rev.* 131 (1963) 1170–1176.
- [5] R. W. P. McWhirter, Ch. 5, in: R. H. Huddleston (Ed.), *Plasma diagnostic techniques*, Academic, New York, 1965, pp. 201–264.
- [6] H. W. Drawin, Validity conditions for local thermodynamic equilibrium, *Z. Phys.* 228 (1969) 99–119.
- [7] W. L. Wiese, H. F. Berg, H. R. Griem, Measurements of temperatures and densities in shock-heated hydrogen and helium plasmas, *Phys. Rev.* 120 (1960) 1079–1085.
- [8] C. A. Bye, A. Scheeline, Saha-Boltzmann statistics for determination of electron-temperature and density in spark discharges using an echelle CCD system, *Appl. Spectrosc.* 47 (1993) 2022–2030.
- [9] T. Belmonte, C. Noël, T. Gries, J. Martin, G. Henrion, Theoretical background of optical emission spectroscopy for analysis of atmospheric pressure plasmas, *Plasma Sources Sci. Technol.* 24 (2015) 064003 1–29.
- [10] J. Glasser, J. Chapelle, J. C. Boettner, Abel inversion applied to plasma spectroscopy - new interactive method, *Appl. Opt.* 17 (1978) 3750–3754.
- [11] R. G. Meyerand, A. F. Haught, Optical-energy absorption and high-density plasma production, *Phys. Rev. Lett.* 13 (1964) 7–9.
- [12] J. Dawson, P. Kaw, B. Green, Optical absorption and expansion of laser-produced plasmas, *Phys. Fluids* 12 (1969) 875.
- [13] F. Brech, L. Cross, *Appl. Spectrosc.* 16 (1962) 59.
- [14] J. Debras-Guédon, N. Liodec, C. R. Acad. Sci. 257 (1963) 3336–3339.
- [15] D. W. Hahn, N. Omenetto, Laser-induced breakdown spectroscopy (LIBS), Part II: Review of instrumental and methodological approaches to material analysis and applications to different fields, *Appl. Spectrosc.* 66 (2012) 347–419.
- [16] R. Noll (Ed.), *Laser-induced breakdown spectroscopy: fundamentals and applications*, Springer, Berlin, 2012.
- [17] L. Mercadier, J. Hermann, C. Grisolia, A. Semerok, Plume segregation observed in hydrogen and deuterium containing plasmas produced by laser ablation of carbon fiber tiles from a fusion reactor, *Spectrochim. Acta Part B: Atom. Spectrosc.* 65 (2010) 715–720.
- [18] G. Cristoforetti, A. De Giacomo, M. Dell’Aglia, S. Legnaioli, E. Tognoni, V. Palleschi, N. Omenetto, Local thermodynamic equilibrium in laser-induced breakdown spectroscopy: beyond the McWhirter criterion, *Spectrochim. Acta Part B: Atom. Spectrosc.* 65 (2010) 86–95.
- [19] A. De Giacomo, J. Hermann, Laser-induced plasma emission: from atomic to molecular spectra, *J. Phys. D: Appl. Phys.* 50 (2017) 183002 1–17.
- [20] C. Aragón, P. Vega, J. Aguilera, Stark width measurements of Fe II lines with wavelengths in the range 260–300 nm, *J. Phys. B* 44 (2011) 55002 1–7.
- [21] M. Cirisan, M. Cvejić, M. R. Gavrilović, S. Jovicević, N. Konjević, J. Hermann, Stark broadening measurement of Al II lines in a laser-induced plasma, *J. Quant. Spectrosc. Radiat. Transfer* 133 (2014) 652–662.
- [22] M. Burger, J. Hermann, Stark broadening measurements in plasmas produced by laser ablation of hydrogen containing compounds, *Spectrochim. Acta Part B: Atom. Spectrosc.* 122 (2016) 118–126.
- [23] M. Ivković, N. Konjević, Stark width and shift for electron number density diagnostics of low temperature plasma: Application to silicon LIBS, *Spectrochim. Acta Part B: Atom. Spectrosc.* 131 (2017) 79–92.
- [24] Y. B. Zel’dovich, Y. P. Raizer, *Physics of shock waves and high temperature phenomena*, Academic, New York, 1966.
- [25] J. Hermann, D. Grojo, E. Axente, C. Gerhard, M. Burger, V. Craciun, Ideal radiation source for plasma spectroscopy generated by laser ablation, *Phys. Rev. E* 96 (2017) 053210 1–6.
- [26] J. Hermann, D. Grojo, E. Axente, V. Craciun, Local thermodynamic equilibrium in a laser-induced plasma evidenced by blackbody radiation, *Spectrochim. Acta Part B: Atom. Spectrosc.* 144 (2018) 82–86.
- [27] J. Hermann, C. Gerhard, E. Axente, C. Dutouquet, Comparative investigation of laser ablation plumes in air and argon by analysis of spectral line shapes: insights on calibration-free laser-induced breakdown spectroscopy, *Spectrochim. Acta Part B: Atom. Spectrosc.* (2014) 189–196.
- [28] J. Hermann, E. Axente, F. Pelascini, V. Craciun, Analysis of multi-elemental thin films via calibration-free laser-induced breakdown spectroscopy, *Anal. Chem.* 91 (2019) 2544–2550.
- [29] C. Gerhard, A. Taleb, F. Pelascini, J. Hermann, Quantification of surface contamination on optical glass via sensitivity-improved calibration-free laser-induced breakdown spectroscopy, *Appl. Surf. Sci.* 537 (2021) 147984 1–7.
- [30] J. Hermann, A. Lorusso, A. Perrone, F. Straffella, C. Dutouquet, B. Torralba, Simulation of emission spectra from nonuniform reactive laser-induced plasmas, *Phys. Rev. E* 92 (2015) 053103 1–15.
- [31] G. Kirchoff, Ueber das Verhältniss zwischen dem Emissionsvermögen und dem Absorptionsvermögen der Körper für Wärme und Licht, *Annalen der Physik* 109 (1860) 275–301.
- [32] X. Z. Zhao, L. J. Shen, T. X. Lu, K. Niemax, Spatial distributions of electron density in microplasmas produced by laser ablation of solids, *Appl. Phys. B: Photophys. Laser Chem.* 55 (1992) 327–330.
- [33] H. R. Griem, *Spectral line broadening of plasmas*, Academic, New York, 1974.
- [34] N. Konjević, J. R. Roberts, A critical review of the Stark widths and shifts of spectral lines from non-hydrogenic atoms, *J. Phys. Chem. Ref. Data* 5 (1976) 209–257.
- [35] R. D. Cowan, G. H. Dieke, Self-absorption of spectrum lines, *Rev. Mod. Phys.* 20 (1948) 418–455.
- [36] J. Hermann, C. Boulmer-Leborgne, D. Hong, Diagnostics of the early phase of an ultraviolet laser induced plasma by spectral line analysis considering self-absorption, *J. Appl. Phys.* 83 (1998) 691–696.
- [37] A. Ciucci, M. Corsi, V. Palleschi, S. Rastelli, A. Salvetti, E. Tognoni, New procedure for quantitative elemental analysis by laser-induced plasma spectroscopy, *Appl. Spectrosc.* 53 (1999) 960–964.
- [38] E. Tognoni, G. Cristoforetti, S. Legnaioli, V. Palleschi, Calibration-free laser-induced breakdown spectroscopy: state of the art, *Spectrochim. Acta Part B: Atom. Spectrosc.* 65 (2010) 1–14.
- [39] E. Tognoni, G. Cristoforetti, S. Legnaioli, V. Palleschi, A. Salvetti, M. Mueller, U. Panne, I. Gomushkin, A numerical study of expected accuracy and precision in calibration-free laser-induced breakdown spectroscopy in the assumption of ideal analytical plasma, *Spectrochim. Acta Part B: Atom. Spectrosc.* 62 (2007) 1287–1302.
- [40] X. L. Mao, A. C. Ciocan, R. E. Russo, Preferential vaporization during laser ablation inductively coupled plasma atomic emission spectroscopy, *Appl. Spectrosc.* 52 (1998) 913–918.
- [41] J. Hermann, L. Mercadier, E. Mothe, G. Socol, P. Alloncle, On the stoichiometry of mass transfer from solid to plasma during pulsed laser ablation of brass, *Spectrochim. Acta Part B: Atom. Spectrosc.* 65 (2010) 636–641.
- [42] G. Cristoforetti, E. Tognoni, L. A. Gizzi, Thermodynamic equi-

- librium states in laser-induced plasmas: From the general case to laser-induced breakdown spectroscopy plasmas, *Spectrochim. Acta Part B: Atom. Spectrosc.* 90 (2013) 1–22.
- [43] C. Gerhard, J. Hermann, L. Mercadier, L. Loewenthal, E. Axente, C. R. Luculescu, T. Sarnet, M. Sentis, W. Viöl, Quantitative analyses of glass via laser-induced breakdown spectroscopy in argon, *Spectrochim. Acta Part B: Atom. Spectrosc.* 101 (2014) 32–45.
- [44] T. Takahashi, B. Thornton, Quantitative methods for compensation of matrix effects and self-absorption in laser induced breakdown spectroscopy signals of solids, *Spectrochim. Acta Part B: Atom. Spectrosc.* 138 (2017) 31–42.
- [45] K. Touchet, F. Chartier, J. Hermann, J. Sirven, Laser-induced breakdown self-reversal isotopic spectrometry for isotopic analysis of lithium, *Spectrochim. Acta Part B: Atom. Spectrosc.* 168 (2020) 105868 1–7.
- [46] V. Lazic, R. Barbini, F. Colao, R. Fantoni, A. Palucci, Self-absorption model in quantitative laser induced breakdown spectroscopy measurements on soils and sediments, *Spectrochim. Acta Part B: Atom. Spectrosc.* 56 (2001) 807–820.
- [47] D. Bulajic, M. Corsi, G. Cristoforetti, S. Legnaioli, V. Palleschi, A. Salvetti, E. Tognoni, A procedure for correcting self-absorption in calibration-free laser-induced breakdown spectroscopy, *Spectrochim. Acta Part B: Atom. Spectrosc.* 57 (2002) 339–353.
- [48] A. M. E. Sherbini, T. M. E. Sherbini, H. Hegazy, G. Cristoforetti, S. Legnaioli, V. Palleschi, L. Pardini, A. Salvetti, E. Tognoni, Evaluation of self-absorption coefficients of aluminum emission lines in laser-induced breakdown spectroscopy measurements, *Spectrochim. Acta Part B: Atom. Spectrosc.* 60 (2005) 1573–1579.
- [49] C. A. D'Angelo, D. M. D. Pace, G. Bertuccelli, D. Bertuccelli, Laser induced breakdown spectroscopy on metallic alloys: Solving inhomogeneous optically thick plasmas, *Spectrochim. Acta Part B: Atom. Spectrosc.* 63 (2008) 367–374.
- [50] J. Hermann, System and method for quantitative analysis of the elemental composition of a material by laser-induced breakdown spectroscopy (LIBS), Patent US8942927 B2.
- [51] R. Wester, R. Noll, Heuristic modeling of spectral plasma emission for laser-induced breakdown spectroscopy, *J. Appl. Phys.* 106 (2009) 123302 1–10.
- [52] J. D. Pedarnig, P. Kolmhofer, N. Huber, B. Praher, J. Heitz, R. Roessler, Element analysis of complex materials by calibration-free laser-induced breakdown spectroscopy, *Appl. Phys. A: Mat. Sci. Proc.* 112 (2013) 105–111.
- [53] M. Dell'Aglio, M. Lopez-Claros, J. J. Laserna, S. Longo, A. De Giacomo, Stand-off laser induced breakdown spectroscopy on meteorites: calibration-free approach, *Spectrochim. Acta Part B: Atom. Spectrosc.* 147 (2018) 87–92.
- [54] G. H. Cavalcanti, D. V. Teixeira, S. Legnaioli, G. Lorenzetti, L. Pardini, V. Palleschi, One-point calibration for calibration-free laser-induced breakdown spectroscopy quantitative analysis, *Spectrochim. Acta Part B: Atom. Spectrosc.* 87 (2013) 51–56.
- [55] R. Gaudiuso, M. Dell'Aglio, O. D. Pascale, S. Loperfido, A. Mangone, A. De Giacomo, Laser-induced breakdown spectroscopy of archaeological findings with calibration-free inverse method: comparison with classical laser-induced breakdown spectroscopy and conventional techniques, *Anal. Chim. Acta* 813 (2014) 15–24.
- [56] C. Aragón, J. A. Aguilera, Direct analysis of aluminum alloys by CSigma laser-induced breakdown spectroscopy, *Anal. Chim. Acta* 1009 (2018) 12–19.
- [57] A. Taleb, V. Motto-Ros, M. J. Carru, E. Axente, V. Craciun, F. Pelascini, J. Hermann, Measurement error due to self-absorption in calibration-free laser-induced breakdown spectroscopy, *Anal. Chim. Acta* 1185 (2021) 339070 1–7.
- [58] A. Taleb, C. Shen, D. Mory, K. Cieřlik, S. Merk, M. R. Aziz, A. P. Caricato, C. Gerhard, F. Pelascini, J. Hermann, Echelle spectrometer calibration by means of laser plasma, *Spectrochim. Acta Part B: Atom. Spectrosc.* 178 (2021) 106144 1–13.
- [59] I. B. Gornushkin, A. Y. Kazakov, N. Omenetto, B. W. Smith, J. D. Winefordner, Experimental verification of a radiative model of laser-induced plasma expanding into vacuum, *Spectrochim. Acta Part B: Atom. Spectrosc.* 60 (2005) 215–230.
- [60] P. Hansen, S. Schröder, S. Kubitzka, K. Rammelkamp, D. Vogt, H.-W. Hübers, Modeling of time-resolved LIBS spectra obtained in Martian atmospheric conditions with a stationary plasma approach, *Spectrochim. Acta Part B: Atom. Spectrosc.* 178 (2021) 106115 1–14.
- [61] J. A. Aguilera, C. Aragón, G. Cristoforetti, E. Tognoni, Application of calibration-free laser-induced breakdown spectroscopy to radially resolved spectra from a copper-based alloy laser-induced plasma, *Spectrochim. Acta Part B: Atom. Spectrosc.* 64 (2009) 685–689.
- [62] K. K. Herrera, E. Tognoni, N. Omenetto, B. W. Smith, J. D. Winefordner, Semi-quantitative analysis of metal alloys, brass and soil samples by calibration-free laser-induced breakdown spectroscopy: recent results and considerations, *J. Anal. At. Spectrom.* 24 (2009) 413–425.
- [63] B. Praher, V. Palleschi, R. Viskup, J. Heitz, J. D. Pedarnig, Calibration free laser-induced breakdown spectroscopy of oxide materials, *Spectrochim. Acta Part B: Atom. Spectrosc.* 65 (2010) 671–679.
- [64] I. B. Gornushkin, T. Völker, A. Y. Kazakov, Extension and investigation by numerical simulations of algorithm for calibration-free laser induced breakdown spectroscopy, *Spectrochim. Acta Part B: Atom. Spectrosc.* 147 (2018) 149–163.
- [65] C.-T. Chen, D. Banaru, T. Sarnet, J. Hermann, Two-step procedure for trace element analysis in food via calibration-free laser-induced breakdown spectroscopy, *Spectrochim. Acta Part B: Atom. Spectrosc.* 150 (2018) 77–85.
- [66] L. Mercadier, A. Semerok, P. A. Kizub, A. V. Leontyev, J. Hermann, C. Grisolia, P. Y. Thro, In-depth analysis of ITER-like samples composition using laser-induced breakdown spectroscopy, *J. Nucl. Mater.* 414 (2011) 485–491.
- [67] J. J. Maali, S. V. Shabanov, Error analysis in optimization problems relevant for calibration-free laser-induced breakdown spectroscopy, *J. Quant. Spectrosc. Radiat. Transf.* 222 (2019) 236–246.
- [68] T. Li, Z. Hou, Y. Fu, J. Yu, W. Gu, Z. Wang, Correction of self-absorption effect in calibration-free laser-induced breakdown spectroscopy (CF-LIBS) with blackbody radiation reference, *Anal. Chim. Acta* 1058 (2019) 39–47.
- [69] I. B. Gornushkin, J. M. Anzano, L. A. King, B. W. Smith, N. Omenetto, J. D. Winefordner, Curve of growth methodology applied to laser-induced plasma emission spectroscopy, *Spectrochim. Acta Part B: Atom. Spectrosc.* 54 (1999) 491–503.
- [70] N. Konjević, A. Lesage, J. R. Führ, W. L. Wiese, Experimental Stark widths and shifts for spectral lines of neutral and ionized atoms (A critical review of selected data for the period 1989 through 2000), *J. Phys. Chem. Ref. Data* 31 (2002) 819–921.
- [71] J. Hermann, E. Axente, V. Craciun, A. Taleb, F. Pelascini, Evaluation of pressure in a plasma produced by laser ablation of steel, *Spectrochim. Acta Part B: Atom. Spectrosc.* 143 (2018) 63–70.
- [72] J. Hermann, Calibration-free laser-induced breakdown spectroscopy, in: V. K. Singh, D. K. Tripathi, Y. Deguchi, Z. Wang (Eds.), *Laser-Induced Breakdown Spectroscopy (LIBS): Concepts, Instrumentation, Data Analysis and Applications*, Wiley,

- Hoboken, 2023, to be published.
- [73] H. Becker-Ross, M. Okruss, S. Florek, U. Heitmann, M. D. Huang, Echelle-spectrograph as a tool for studies of structured background in flame atomic absorption spectrometry, *Spectrochim. Acta Part B: Atom. Spectrosc.* 57 (2002) 1493–1504.
  - [74] A. Kramida, Y. Ralchenko, J. Reader, NIST Atomic Spectra Database (version 5.8), National Institute of Standards and Technology, Gaithersburg, MD (2020).  
URL <http://physics.nist.gov/PhysRefData/ASD/>
  - [75] P. L. Smith, C. Heise, J. R. Esmond, R. L. Kurucz, Atomic spectral line database built from atomic data files from R. L. Kurucz CD-ROM 23 (2011).  
URL [www.pmp.uni-hannover.de/cgi-bin/ssi/test/kurucz/sekur.html](http://www.pmp.uni-hannover.de/cgi-bin/ssi/test/kurucz/sekur.html)
  - [76] N. Konjević, M. S. Dimitrijević, W. L. Wiese, Experimental Stark widths and shifts for spectral lines of neutral atoms (A critical review of selected data for the period 1976 to 1982), *J. Phys. Chem. Ref. Data* 13 (1984) 619–647.
  - [77] N. Konjević, Plasma broadening and shifting of non-hydrogenic spectral lines: present status and applications, *Phys. Rep.* 316 (1999) 339–401.
  - [78] A. Lesage, Experimental Stark widths and shifts for spectral lines of neutral and ionized atoms. A critical review of selected data for the period 2001–2007, *New Astron. Rev.* 52 (2009) 471–535.
  - [79] H. Griem, Stark broadening of the hydrogen Balmer- $\alpha$  line in low and high density plasmas, *Contrib. Plasma Phys.* 40 (2000) 46–56.
  - [80] M. A. Gigosos, M. A. Gonzalez, V. Cardenoso, Computer simulated Balmer-alpha, -beta, and -gamma Stark line profiles for non-equilibrium plasma diagnostics, *Spectrochim. Acta Part B: Atom. Spectrosc.* 58 (2003) 1489–1504.
  - [81] S. Zielinska, S. Pellerin, K. Dzierzega, F. Valensi, K. Musiol, F. Briand, Measurement of atomic Stark parameters of many Mn I and Fe I spectral lines using GMAW process, *J. Phys. D: Appl. Phys.* 43 (2010) 434005 1–10.
  - [82] A. Alonso-Medina, A spectroscopic study of laser-induced tin-lead plasma: transition probabilities for spectral lines of Sn I, *Spectrochim. Acta Part B: Atom. Spectrosc.* 65 (2010) 158–166.